Available online at www.eccomasproceedia.org
Eccomas Proceedia COMPDYN (2023) 4174-4188

ECCOMAS
Proceedia

COMPDYN 2023
9th ECCOMAS Thematic Conference on
Computational Methods in Structural Dynamics and Earthquake Engineering
M. Papadrakakis, M. Fragiadakis (eds.)
Athens, Greece, 12-14 June 2023

MULTISCALE MODELING OF COUPLED THERMO-HYDRO-MECHANICAL ANALYSIS OF HETEROGENEOUS POROUS MEDIA WITH MICRO-DYNAMIC EFFECTS

Amir R. Khoei and Saeed Saeedmonir

Center of Excellence in Structures and Earthquake Engineering, Department of Civil Engineering,
Sharif University of Technology, P.O. Box. 11365-9313, Tehran, Iran
e-mail: arkhoei@sharif.edu

Abstract

This paper presents a computational multiscale model for analysis of the transient heat and fluid flow in deformable porous media. Because of the heterogeneity in the porous media, the direct numerical simulation (DNS) of the micro-structures leads to high computational costs. Hence, the multiscale technique is developed to provide an efficient computational procedure. Accordingly, the first-order computational homogenization method is applied for two-scale simulation of THM problems. The Hill-Mandel theory is extended to capture the presence of micro-dynamic effects. The governing equations of the THM problem include the stress equilibrium equation, the mass continuity equation, and the advection-diffusion equation in a fully coupled manner. The weak forms of governing equations are then obtained as a bridging stage between the scales. Different boundary conditions of the microscopic domain are defined in terms of the macroscopic information to fulfill the averaging constraints. In order to consider the transient dynamic effects, the micro-inertial terms are involved in the micro-scale analysis, and the microscopic boundary conditions are improved to evaluate the accuracy of the analysis. The macroscopic properties including the homogenized tangent material property tensor and equivalent quantities, such as stress tensors, are determined from the microscopic solution through the appropriate mathematical approaches. Moreover, an upwind finite element squared method is employed for highly advective heat transfer to achieve the accurate spatial results. Finally, the numerical example of 2D heterogeneous medium is simulated to study the efficiency and validity of the proposed computational algorithm.

Keywords: Computational homogenization, THM analysis, Micro-dynamic effects, Heterogeneous porous media, Advection-diffusion.

ISSN:2623-3347 © 2023 The Authors. Published by Eccomas Proceedia.
Peer-review under responsibility of the organizing committee of COMPDYN 2023.
doi: 10.7712/120123.10710.21137

1 INTRODUCTION

There are several engineering problems that include the coupling of different physics, such as hydraulic fracturing, cold and hot water injection in reservoirs, oil and gas reservoirs, radioactive waste disposal, geothermal reservoirs, ground energy storage systems and etc. There are various numerical methods developed in the literature to simulate the coupled thermo-hydro-mechanical (THM) problems in steady-state and transient conditions [1–6], the multi-phase flow systems [7, 8], and the fractured thermo-hydro-mechanical media [9–12]. In real engineering problems, the case studies are generally constructed from complex micro-heterogeneities, resulting in high computational cost for modeling the micro-structures in details. Hence, the multiscale techniques have been developed by researchers to reduce the computational cost of numerical simulation without the compensation of accuracy. Among all multiscale approaches, the computational homogenization technique is found efficient and applicable to various problems. Computational homogenization approach is an interesting method in study of complex problems. In this method, the two scale levels are considered as the micro-scale and macro-scale levels, in which the constitutive behavior and equivalent quantities of each scale is determined through the solution of the lower scale. Since the heterogeneities are not directly modeled in the coarse-scale domain, this procedure reduces the computational cost as the analysis is performed distinctly for each micro-scale domain; hence, the high CPU and memory storage are not crucial in this approach.

In the computational homogenization method, the micro-scale and macro-scale are solved simultaneously with the finite element method, called the FE^2, with the information transferring between the two scales continuously. In the micro-scale level, a sample domain, called as the Representative Volume Element (RVE), is determined and simulated subject to specific boundary conditions, developed from the macro-scale level [13]. Basically, selection of the RVE is a significant step in the multiscale analysis and has been one of the major concerns by researchers [14, 15]. In fact, the micro-scale characteristic length for the RVE must be much smaller than the macro-scale level of the continuum model, which is an important assumption in the multiscale analysis, which is called the principle of separation of scales. However, the size and configuration of a RVE must be defined according to the distribution and arrangement of heterogeneities in the natural system. Moreover, the RVE size should be defined in a manner that an increase in the RVE size causes no change in the overall results of the simulation [16]. The RVE must represent even the smallest heterogeneity, so selection of the RVE is a significant step in the multiscale analysis.

In the present paper, a two-scale model is developed for the thermo-hydro-mechanical analysis of heterogeneous porous media. The transient dynamic effects of micro-structures are taken into account. The computational homogenization technique is developed based on the finite element squared method (FE^2), in which a Representative Volume Element is associated with each Gauss point of a macroscopic domain as the microscopic domain. For micro-scale analysis of the RVE, the appropriate boundary conditions are considered including the periodic and linear boundary conditions. In order to take the micro-inertial terms into account, additional constraints are coupled with the conventional periodic boundary conditions. Note that in the advection-diffusion equation coupled with the hydro-mechanical equations, the transient behavior of the micro-scale domain is not similar to the pure conduction problem. In fact, the presence of the convection (advection) heat transfer leads to numerical errors when the fluid velocity takes a large value. Thus, the Petrov-Galerkin finite element method is employed in the micro-scale domain instead of the conventional Galerkin FE method for the

weak formulation of the advection-diffusion equation. However, there are alternative techniques, such as the artificial diffusion method that lead to the same solution. It is demonstrated that on the contrary to the single-scale simulation, often called the Direct Numerical Simulation (DNS), the multiscale analysis does not lead to oscillating behavior in the spatial discretization of temperature field in highly convective problems.

2 GOVERNING EQUATIONS OF THM PROBLEM

The governing equations of THM problem are derived for two continuum scales of the multiscale analysis, in which the micro-scale, which is called the microscopic level, contains the heterogeneities of the medium, and the macroscopic scale is assumed as the homogenized domain of the physical problem. The governing equations are solved at the micro-scale level according to the specific boundary conditions, which is derived from the macroscopic level. In fact, a microscopic domain is associated with each material point of the macroscopic domain, where the macroscopic data are downscaled to the micro-scale level. The required data are then upscaled to the macro-scale level through the well-known Hill-Mandel principle of macro-homogeneity. In this study, the first order homogenization method is adopted, so the macroscopic main variables and their gradient fields are downscaled to the microscopic level. It must be noted that the classical separation of scales may need some reconsiderations in the case of transient loading [17, 18]. In such case, the full separation of scales cannot be considered anymore and the transient terms in the micro-scale level have significant influence on the overall transient behavior of the macroscopic problem. In this manner, the transient computational homogenization should be utilized to capture the micro-dynamic effects. In what follows, the governing equations of the thermo-hydro-mechanical analysis are presented.

In this study, the macroscopic quantities and mathematical operations with respect to the macroscopic coordinates are indicated by a bar, e.g. $\overline{\Theta}$. Hence, a quantity without a bar represents a microscopic quantity or operation with respect to microscopic coordinates. In addition, quantities with a tilde sign on top, e.g. $\tilde{\Theta}$, show the fluctuation field in the RVE. The volume average of a quantity in a specific domain in the RVE is defined as

$$\langle \Xi \rangle_{\Omega_0} = \frac{1}{|\Omega_0|} \int_{\Omega_0} \Xi \, d\Omega \tag{1}$$

In order to model the non-isothermal flow in a saturated deformable porous medium, the coupled governing equations are presented based on the force equilibrium equation, momentum balance equation, and energy balance equation. Based on the $u-p$ formulation, the primary variables are chosen as the displacement field u, fluid pressure p, and temperature of the mixture θ [19–21]. In this study, the instantaneous thermal equilibrium is considered between the fluid and solid, i.e. $\theta_S = \theta_f$; thus, only one energy balance equation is evaluated. The strong form of the mentioned equations can be expressed as

$$\begin{aligned}
&\boldsymbol{\nabla}.\boldsymbol{\sigma} + \mathbf{f}_{\text{Int}} = \mathbf{0} && \text{with} && \mathbf{f}_{\text{I}} = \rho\mathbf{b} - \rho\ddot{\mathbf{u}} \\
&\boldsymbol{\nabla}.\dot{\mathbf{w}} + \dot{\zeta} = 0 && \text{with} && \dot{\zeta} = \alpha\boldsymbol{\nabla}.\dot{\mathbf{u}} + \frac{\dot{p}}{Q} - \beta_f\dot{\theta} \\
&\nabla.\boldsymbol{J} + \dot{\eta}' = 0 && \text{with} && \boldsymbol{J} = \boldsymbol{J}_{\text{adv}} + \boldsymbol{J}_{\text{dif}} \quad \text{and} \quad \eta' = \rho c\theta
\end{aligned} \tag{2}$$

in which $\boldsymbol{\sigma}$ is the total stress tensor defined as $\boldsymbol{\sigma} = \boldsymbol{\sigma}' - \alpha p\mathbf{I}$, with $\boldsymbol{\sigma}'$ denoting the effective stress tensor, $\mathbf{f}_{\text{int}}$ is the inertial force vector, and $\mathbf{b}$ is the body force vector. In above, $\boldsymbol{\sigma}'$ is

defined as $\boldsymbol{\sigma}' = \mathbf{C} : (\boldsymbol{\varepsilon} - \boldsymbol{\varepsilon}_T)$ in the presence of thermal strain, with $\mathbf{C}$ indicating the elasticity tensor. Moreover, $\dot{\mathbf{w}}$, $\dot{\varsigma}$, α, Q and β denote the Darcy velocity vector of the fluid with respect to the solid skeleton, the fluid content per volume, the Biot coefficient, the compressibility coefficient of the mixture, and the thermal expansion of the bulk, respectively. Also, it can be stated $\alpha = 1 - K_T / K_S$, $1/Q = (\alpha - n)/K_S + n/K_f$ and $\beta = (\alpha - n)\beta_s + n\beta_f$, in which K_T, K_S and K_f stand for the bulk modulus of the mixture, solid grains and fluid, respectively, and n is the porosity of the soil. It is noteworthy that β_s and β_f are the thermal expansion coefficients of the solid and fluid, respectively. For plane strain problems, β_s should be replaced by $\beta_s' = \beta_s(1+\nu)$, with ν denoting the Poisson ratio. In above equations, the average density of the mixture is defined as $\rho = (1-n)\rho_s + n\rho_f$. The term $\dot{\varsigma}$ in the 2nd equation of governing equations (2) can be obtained from the change of fluid density, which is described as $\rho_f = \rho_{f_0} \exp\left[-\beta_f \theta + 1/K_f (p - p_0)\right]$ [22]. In addition, $\boldsymbol{J}$, $\dot{\eta}'$ and c are respectively the total heat flux vector, heat content per volume and specific heat capacity. For a solid-fluid mixture, the average heat capacity is defined as $\rho c = (1-n)(\rho c)_s + n(\rho c)_f$. The 3rd equation of governing equations (2) is the Divergence form of the advection-diffusion equation [23]. Due to the presence of the fluid flow, the heat is transferred by both conduction (diffusion) and convection (advection) regimes. It should be noted that the total energy balance equation is derived from the combination of the energy balance equation for each phase. Applying the Fourier law of thermal conduction, the advective and diffusive heat fluxes can be obtained as

$$\begin{aligned} \boldsymbol{J}_{\text{adv}} &= (\rho c)_f \dot{\mathbf{w}} \theta \\ \boldsymbol{J}_{\text{dif}} &= -\lambda \boldsymbol{\nabla} \theta \end{aligned} \tag{3}$$

where λ is the average conductivity (diffusivity) of the mixture, defined as $\lambda = (1-n)\lambda_s + n\lambda_f$. Expanding the 3rd equation of governing equations (2) and applying equation (3) and the mass continuity equations of the solid and fluid phases, the convective form of the energy balance equation can be extracted as

$$\boldsymbol{\nabla}.(\boldsymbol{J}_{\text{dif}}) + \eta = 0 \qquad \text{with} \qquad \eta = (\rho c)_f \dot{\mathbf{w}} \boldsymbol{\nabla} \theta + \rho c \dot{\theta} \tag{4}$$

where $\boldsymbol{J}_{\text{dif}} = -\lambda \nabla \theta$. It should be noted that in the convective form, η cannot be taken as the previously defined heat content and the effect of advection must be included. The fluid relative velocity $\dot{\mathbf{w}}$ can be obtained from the generalized Darcy law by $\dot{\mathbf{w}} = \mathbf{k}(-\nabla p + \rho \mathbf{b} - \rho \ddot{\mathbf{u}})$, with $\mathbf{k}$ denotes the permeability tensor of the porous medium. It is noted that the convective form of the advection-diffusion equation neglects the explicit dependency of the equation to the displacement and pressure fields, while in the Divergence form, all the main variables are included in the equation.

3 MULTISCALE FORMULATION OF THM PROBLEMS

In order to perform the multiscale analysis of THM problem, the method of multiple scales is carried out, in which a macroscopic domain is considered as the homogenized medium and a micro-scale domain is assigned to each material point. In this manner, the homogenized quantities are extracted from the micro-scale domain at each material point employing the two scale transitions within the multiscale analysis; first downscaling the macroscopic solution to the micro-scale and then, upscaling the homogenized quantities to the macro-scale problem.

3.1 Downscaling technique

Let Ω and Γ denote the domain and the boundary of the Representative Volume Element (RVE) at the micro-scale domain, respectively. The primary fields at the RVE can be described as

$$\begin{aligned} \mathbf{u}(\mathbf{x}) &= \bar{\mathbf{u}} + \bar{\boldsymbol{\nabla}}\bar{\mathbf{u}}.\mathbf{x} + \tilde{\mathbf{u}} \equiv \bar{\mathbf{u}} + \mathbf{H}^{\mathrm{T}}\bar{\boldsymbol{\epsilon}} + \tilde{\mathbf{u}} \qquad \text{with} \qquad \mathbf{H} = \begin{bmatrix} x_1 & 0 & x_2/2 \\ 0 & x_2 & x_1/2 \end{bmatrix} \\ p(\mathbf{x}) &= \bar{p} + \mathbf{x}^{\mathrm{T}}\,\bar{\boldsymbol{\nabla}}\bar{p} + \tilde{p} \\ \theta(\mathbf{x}) &= \bar{\theta} + \mathbf{x}^{\mathrm{T}}\,\bar{\boldsymbol{\nabla}}\bar{\theta} + \tilde{\theta} \end{aligned} \tag{5}$$

in which $\mathbf{x} \in \Omega$ is the position vector of a point in the RVE, measured from the centroid of the RVE. It should be noted that the first two terms of the above relations are known as the smooth part of the microscopic fields, which vary linearly inside the RVE, and the third terms, which are known as the fluctuation fields, play the role of higher order terms in the Taylor expansion of the functions. These terms are the variable parts of the solution defined through the micro-scale analysis. In addition, it is noteworthy that for displacement field, the Voigt notation can be exploited for the simplicity of the finite element formulation as an alternative to the general formulation in terms of displacement gradient (or deformation gradient). As a basic assumption in the homogenization framework, the average of gradient fields should be equal to the macroscopic gradients. Hence, the following constraints can be written as

$$\begin{aligned} \bar{\boldsymbol{\epsilon}} &= \frac{1}{|\Omega|}\int_{\Omega} \boldsymbol{\epsilon}\, d\Omega \\ \bar{\boldsymbol{\nabla}}\bar{p} &= \frac{1}{|\Omega|}\int_{\Omega} \boldsymbol{\nabla} p\, d\Omega \\ \bar{\boldsymbol{\nabla}}\bar{\theta} &= \frac{1}{|\Omega|}\int_{\Omega} \boldsymbol{\nabla}\theta\, d\Omega \end{aligned} \tag{6}$$

As a result of equations (5) and (6), it can be stated that

$$\begin{aligned} \int_{\Gamma} \boldsymbol{\mathcal{N}}\tilde{\mathbf{u}}\, d\Gamma &= \mathbf{0} \qquad \text{with} \qquad \boldsymbol{\mathcal{N}} = \begin{bmatrix} n_1 & 0 & n_2 \\ 0 & n_2 & n_1 \end{bmatrix}^{T} \\ \int_{\Gamma} \tilde{p}\,\mathbf{n}\, d\Gamma &= 0 \\ \int_{\Gamma} \tilde{\theta}\,\mathbf{n}\, d\Gamma &= 0 \end{aligned} \tag{7}$$

where $\mathbf{n}$ is the outward normal vector at the boundary of the RVE. It must be noted that in the above procedure, the Green theorem is employed to transform the domain integral equation to a boundary integral equation. In order to satisfy the aforementioned constraints, various techniques have been proposed in the literature, such as the Taylor model, linear boundary condition, periodic boundary condition, minimally constrained boundary condition, and Reuss methods. Among all these approaches, the periodic boundary condition is known to exhibit the closest response to the exact ones in comparison to the other techniques. Hence, the periodic boundary condition is chosen here to study the proposed computational algorithm. In this method, the fluctuation fields at the opposite boundaries of the RVE are set to be equal, which

results in anti-periodic tractions and fluxes. Moreover, to maintain the magnitude of volume average of the field variables to the macroscopic solution, four corner points are constrained such that the fluctuation fields vanish in these points.

3.2 Upscaling technique

In order to perform the multiscale analysis, the required variables should be extracted from the micro-scale solution and utilized in the macro-scale solution. To this end, an extended form of the Hill-Mandel principle of macro-homogeneity is adopted [24, 25]. According to this principle, the volume average of the virtual power in the microscopic domain should be equal to the macroscopic virtual power at the associated point. From the weak form of the governing equations (2) and (4), the volume average of the virtual work can be expressed in the microscopic domain as

$$\begin{aligned}
\langle \delta \mathcal{W}^u \rangle &:= \frac{1}{|\Omega|}\int_\Omega (\delta \boldsymbol{\nabla}\mathbf{u}: \boldsymbol{\sigma} - \delta \mathbf{u}.(\rho \mathbf{b} - \rho \ddot{\mathbf{u}}))\, d\Omega \\
\langle \delta \mathcal{W}^f \rangle &:= \frac{1}{|\Omega|}\int_\Omega \Big(-\delta \boldsymbol{\nabla} p.\dot{\mathbf{w}} + \delta p\, \alpha\, \boldsymbol{\nabla}.\dot{\mathbf{u}} + \delta p \frac{\dot{p}}{Q} - \delta p\, \beta_f \dot{\theta} \Big)\, d\Omega \\
\langle \delta \mathcal{W}^\theta \rangle &:= \frac{1}{|\Omega|}\int_\Omega \big(- \delta \boldsymbol{\nabla}\theta.\boldsymbol{J}_{\text{dif}} + \delta\theta (\rho c)_f \dot{\mathbf{w}}.\boldsymbol{\nabla}\theta + \delta\theta\, \rho c \dot{\theta} \big) d\Omega
\end{aligned} \tag{8}$$

in which for the corresponding material point in the macroscopic domain, the virtual work relations can be described as

$$\begin{aligned}
\delta \bar{\mathcal{W}}^u &:= \delta \bar{\boldsymbol{\nabla}}\bar{\mathbf{u}}: \bar{\boldsymbol{\sigma}} - \delta \bar{\mathbf{u}}.\big(\bar{\rho}\bar{\mathbf{b}} - \bar{\rho}\ddot{\bar{\mathbf{u}}}\big) = \delta \bar{\boldsymbol{\nabla}}\bar{\mathbf{u}}: \bar{\boldsymbol{\sigma}} - \delta \bar{\mathbf{u}}.\bar{\mathbf{f}}_{\text{Int}} \\
\delta \bar{\mathcal{W}}^f &:= -\delta \bar{\boldsymbol{\nabla}}\bar{p}.\dot{\bar{\mathbf{w}}} + \delta \bar{p}\, \bar{\alpha}\, \bar{\boldsymbol{\nabla}}.\dot{\bar{\mathbf{u}}} + \delta \bar{p} \frac{\dot{\bar{p}}}{\bar{Q}} - \delta \bar{p}\, \overline{\beta_f}\dot{\bar{\theta}} = -\delta \bar{\boldsymbol{\nabla}}\bar{p}.\dot{\bar{\mathbf{w}}} + \delta \bar{p}\dot{\bar{\zeta}} \\
\delta \bar{\mathcal{W}}^\theta &:= -\delta \bar{\boldsymbol{\nabla}}\bar{\theta}.\bar{\boldsymbol{J}} + \delta \bar{\theta}(\bar{\rho}\bar{c})_f \dot{\bar{\mathbf{w}}}.\boldsymbol{\nabla}\theta + \delta\bar{\theta}\, \bar{\rho}\bar{c}\dot{\bar{\theta}} = -\delta \bar{\boldsymbol{\nabla}}\bar{\theta}.\bar{\boldsymbol{J}} + \delta\bar{\theta}\bar{\eta}
\end{aligned} \tag{9}$$

In order to perform the macro-homogeneity principle, the macroscopic virtual power should be derived from the average of virtual powers in the micro-scale domain. Hence, it can be concluded from equations (8) and (9) that

$$\begin{aligned}
\delta \bar{\boldsymbol{\nabla}}\bar{\mathbf{u}}: \bar{\boldsymbol{\sigma}} - \delta \bar{\mathbf{u}}.\bar{\mathbf{f}}_{\text{Int}} &= \frac{1}{|\Omega|}\int_\Omega (\delta \boldsymbol{\nabla}\mathbf{u}: \boldsymbol{\sigma} - \delta \mathbf{u}.\mathbf{f}_{\text{Int}})\, d\Omega \\
-\delta \bar{\boldsymbol{\nabla}}\bar{p}.\dot{\bar{\mathbf{w}}} + \delta \bar{p}\dot{\bar{\zeta}} &= \frac{1}{|\Omega|}\int_\Omega \big(-\delta \boldsymbol{\nabla} p.\dot{\mathbf{w}} + \delta p\, \dot{\zeta} \big) d\Omega \\
-\delta \bar{\boldsymbol{\nabla}}\bar{\theta}.\bar{\boldsymbol{J}} + \delta\bar{\theta}\bar{\eta} &= \frac{1}{|\Omega|}\int_\Omega \big(- \delta \boldsymbol{\nabla}\theta.\boldsymbol{J}_{\text{dif}} + \delta\theta\, \eta \big) d\Omega
\end{aligned} \tag{10}$$

in which the right-hand sides in above equations are expressed in the forms given in equations (2) and (4). Applying the downscaling relations defined in (5), considering the variations of macroscopic terms, i.e. $\delta\bar{\mathbf{u}}$, $\delta\bar{p}$, and $\delta\bar{\theta}$, as the constant functions within the RVE, and substituting the above relations into the right-hand side of equations (3), it leads to

$$\begin{aligned}
\delta \bar{\boldsymbol{\nabla}}\bar{\mathbf{u}}: \bar{\boldsymbol{\sigma}} - \delta \bar{\mathbf{u}}.\bar{\mathbf{f}}_{\text{Int}} = \delta \bar{\boldsymbol{\nabla}}\bar{\mathbf{u}}: &\left(\frac{1}{|\Omega|}\int_\Omega (\boldsymbol{\sigma} - \mathbf{f}_{\text{Int}} \otimes \mathbf{x})\, d\Omega \right) \\
&- \delta \bar{\mathbf{u}}.\left(\frac{1}{|\Omega|}\int_\Omega \mathbf{f}_{\text{Int}}\, d\Omega \right) + \left(\frac{1}{|\Omega|}\int_\Omega (\delta \boldsymbol{\nabla}\tilde{\mathbf{u}}: \boldsymbol{\sigma} - \delta \tilde{\mathbf{u}}.\mathbf{f}_{\text{Int}})\, d\Omega \right)
\end{aligned}$$

$$
\begin{aligned}
-\delta\bar{\nabla}\bar{p}.\dot{\bar{\mathbf{w}}}+\delta\bar{p}\dot{\bar{\zeta}} &= -\delta\bar{\nabla}\bar{p}.\left(\frac{1}{|\Omega|}\int_{\Omega}(\dot{\mathbf{w}}-\mathbf{x}\,\dot{\zeta})d\Omega\right)\\
&\quad+\delta\bar{p}.\left(\frac{1}{|\Omega|}\int_{\Omega}\dot{\zeta}\,d\Omega\right)+\left(\frac{1}{|\Omega|}\int_{\Omega}(-\delta\nabla\tilde{p}.\dot{\mathbf{w}}+\delta\tilde{p}\,\dot{\zeta})d\Omega\right)\\
-\delta\bar{\nabla}\bar{\theta}.\bar{\boldsymbol{J}}+\delta\bar{\theta}\bar{\eta} &= -\delta\bar{\nabla}\bar{\theta}.\left(\frac{1}{|\Omega|}\int_{\Omega}(\boldsymbol{J}_{\mathrm{dif}}-\mathbf{x}\,\eta)d\Omega\right)\\
&\quad+\delta\bar{\theta}.\left(\frac{1}{|\Omega|}\int_{\Omega}\eta\,d\Omega\right)+\left(\frac{1}{|\Omega|}\int_{\Omega}(-\delta\nabla\tilde{\theta}.\boldsymbol{J}_{\mathrm{dif}}+\delta\tilde{\theta}\,\eta)d\Omega\right)
\end{aligned}
\tag{11}
$$

Applying the Divergence theorem to the third terms at the right-hand side of above equations, it can be concluded that these terms can be vanished by applying the appropriate boundary conditions, e.g. the periodic boundary conditions and linear boundary conditions. These equations can be considered as the variational form of governing equations in the microscopic scale. In fact, the weak forms of the micro-scale problem are recovered directly from the generalized Hill-Mandel principle, which should be solved under the mentioned boundary conditions. On the other hand, by noting the fact that functions $\delta\bar{\nabla}\bar{\mathbf{u}}$, $\delta\bar{\mathbf{u}}$, $\delta\bar{\nabla}\bar{p}$, $\delta\bar{p}$, $\delta\bar{\nabla}\bar{\theta}$, and $\delta\bar{\theta}$ are arbitrary functions, the following results can be achieved from (11) as

$$
\begin{aligned}
\bar{\boldsymbol{\sigma}} &= \frac{1}{|\Omega|}\int_{\Omega}(\boldsymbol{\sigma}-\mathbf{f}_{\mathrm{Int}}\otimes\mathbf{x})\,d\Omega & \bar{\mathbf{f}}_{\mathrm{Int}} &= -\frac{1}{|\Omega|}\int_{\Omega}\mathbf{f}_{\mathrm{Int}}\,d\Omega\\
\dot{\bar{\mathbf{w}}} &= -\frac{1}{|\Omega|}\int_{\Omega}(\dot{\mathbf{w}}-\mathbf{x}\,\dot{\zeta})d\Omega & \dot{\bar{\zeta}} &= \frac{1}{|\Omega|}\int_{\Omega}\dot{\zeta}\,d\Omega\\
\bar{\boldsymbol{J}} &= -\frac{1}{|\Omega|}\int_{\Omega}(\boldsymbol{J}_{\mathrm{dif}}-\mathbf{x}\,\eta)d\Omega & \bar{\eta} &= \frac{1}{|\Omega|}\int_{\Omega}\eta\,d\Omega
\end{aligned}
\tag{12}
$$

Obviously, it can be observed from relations (12) that the macroscopic quantities are extracted from the microscopic solution. However, the classical averaging approach does not hold in the current formulation due to presence of the transient terms.

4 FINITE ELEMENT MODELING OF THM MULTISCALE ANALYSIS

4.1 FE discretization of macro-scale domain

In order to derive the FE discretization of macro-scale governing equations, the weak forms of the macro-scale domain are defined on the basis of information upscaled from the microscopic model. To this end, the variational forms of the macroscopic governing equations can be expressed as

$$
\begin{aligned}
&\int_{\bar{\Omega}}\left(\delta\bar{\nabla}\bar{\mathbf{u}}:\bar{\boldsymbol{\sigma}}-\delta\bar{\mathbf{u}}.\bar{\mathbf{f}}_{\mathrm{Int}}\right)d\Omega-\int_{\bar{\Gamma}}\delta\bar{\mathbf{u}}^{\mathrm{T}}\bar{\mathbf{t}}\;d\Gamma\;=0\\
&\int_{\bar{\Omega}}\left(-\delta\bar{\nabla}\bar{p}.\dot{\bar{\mathbf{w}}}+\delta\bar{p}\dot{\bar{\zeta}}\right)d\Omega+\int_{\bar{\Gamma}}\delta\bar{p}\;\bar{q}_f\;d\Gamma=0\\
&\int_{\bar{\Omega}}(-\delta\bar{\nabla}\bar{\theta}.\bar{\boldsymbol{J}}+\delta\bar{\theta}\bar{\eta})\,d\Omega+\int_{\bar{\Gamma}}\delta\bar{\theta}\;\bar{q}_T\,d\Gamma=0
\end{aligned}
\tag{13}
$$

Applying the finite element discretization, the weak forms of the macro-scale domain can be discretized as

$$\begin{aligned}
\bar{\boldsymbol{\psi}}_u &= \int_{\bar{\Omega}} \left(\bar{\mathbf{B}}_u^{\mathrm{T}}\ \underline{\bar{\boldsymbol{\sigma}}} - \bar{\mathbf{N}}_u^{\mathrm{T}}\ \bar{\mathbf{f}}_{\mathrm{Int}}\right) d\Omega - \int_{\bar{\Gamma}} \bar{\mathbf{N}}_u^{\mathrm{T}}\ \bar{\mathbf{t}}\ d\Gamma\ = 0 \\
\bar{\boldsymbol{\psi}}_p &= \int_{\bar{\Omega}} \left(-\bar{\mathbf{B}}_p^{\mathrm{T}}\ \dot{\bar{\mathbf{w}}} + \bar{\mathbf{N}}_p^{\mathrm{T}}\ \dot{\bar{\zeta}}\right) d\Omega + \int_{\bar{\Gamma}} \bar{\mathbf{N}}_p^{\mathrm{T}}\ \bar{q}_f\ d\Gamma = 0 \\
\bar{\boldsymbol{\psi}}_T &= \int_{\bar{\Omega}} \left(-\bar{\mathbf{B}}_\theta^{\mathrm{T}} \dot{\bar{\boldsymbol{J}}} + \bar{\mathbf{N}}_\theta^{\mathrm{T}}\ \dot{\bar{\eta}}\right) d\Omega + \int_{\bar{\Gamma}} \bar{\mathbf{N}}_\theta^{\mathrm{T}}\ \bar{q}_T\ d\Gamma = 0
\end{aligned} \tag{14}$$

where $\bar{\mathbf{N}}_u$, $\bar{\mathbf{N}}_p$ and $\bar{\mathbf{N}}_\theta$ are the global shape functions corresponding to the primary variables and $\bar{\mathbf{B}}_u$, $\bar{\mathbf{B}}_p$ and $\bar{\mathbf{B}}_\theta$ denote the gradients of the shape functions. In above, the underbar '_" is utilized to represent the vector form of the symmetric 2nd order tensors, such as the stress tensor. Due to the general nonlinearity of equations (14), the Newton-Raphson scheme is adopted in order to linearize and solve the discretized system of governing equations as

$$\bar{\boldsymbol{\mathcal{F}}}_n^{i+1} = \bar{\boldsymbol{\mathcal{F}}}_n^i + \bar{\boldsymbol{\mathcal{J}}}_n^i . d\bar{\boldsymbol{\mathcal{X}}}_n^i \quad , \quad \bar{\boldsymbol{\mathcal{F}}} = \begin{Bmatrix} \bar{\boldsymbol{\psi}}_u \\ \bar{\boldsymbol{\psi}}_p \\ \bar{\boldsymbol{\psi}}_T \end{Bmatrix} \quad , \quad \bar{\boldsymbol{\mathcal{X}}} = \begin{Bmatrix} \bar{\mathbf{U}} \\ \bar{\mathbf{P}} \\ \bar{\boldsymbol{\Theta}} \end{Bmatrix} \tag{15}$$

where $\bar{\boldsymbol{F}}$ is the nodal values of residual vector, $\bar{\boldsymbol{X}}$ denotes the nodal values of the primary variables, and $\bar{\boldsymbol{J}}$ represents the Jacobian matrix defined as

$$\bar{\boldsymbol{\mathcal{J}}} = \begin{bmatrix} \dfrac{\partial \bar{\boldsymbol{\psi}}_u}{\partial \bar{\mathbf{U}}} & \dfrac{\partial \bar{\boldsymbol{\psi}}_u}{\partial \bar{\mathbf{P}}} & \dfrac{\partial \bar{\boldsymbol{\psi}}_u}{\partial \boldsymbol{\Theta}} \\ \dfrac{\partial \bar{\boldsymbol{\psi}}_p}{\partial \bar{\mathbf{U}}} & \dfrac{\partial \bar{\boldsymbol{\psi}}_p}{\partial \bar{\mathbf{P}}} & \dfrac{\partial \bar{\boldsymbol{\psi}}_p}{\partial \boldsymbol{\Theta}} \\ \dfrac{\partial \bar{\boldsymbol{\psi}}_T}{\partial \bar{\mathbf{U}}} & \dfrac{\partial \bar{\boldsymbol{\psi}}_T}{\partial \bar{\mathbf{P}}} & \dfrac{\partial \bar{\boldsymbol{\psi}}_T}{\partial \boldsymbol{\Theta}} \end{bmatrix} \tag{16}$$

In relation (15), the subscripts and superscripts, denoted by n and i, represent the number of increment and iteration, respectively. In equation (16), the components of the Jacobian matrix can be obtained by taking the variations of (13) with respect to the primary variables.

4.2 FE discretization of micro-scale domain

In order to derive the FE discretization of micro-scale governing equations, the weak forms of the micro-scale domain are derived to determine the response of the RVE. The variational formulations of microscopic governing equations can be obtained as

$$\begin{aligned}
&\int_\Omega (\delta \boldsymbol{\nabla} \tilde{\mathbf{u}} : \boldsymbol{\sigma} - \delta \tilde{\mathbf{u}} . (\rho \mathbf{b} - \rho \ddot{\mathbf{u}}))\, d\Omega = 0 \\
&\int_\Omega \left(-\delta \boldsymbol{\nabla} \tilde{p} . \dot{\mathbf{w}} + \delta \tilde{p}\ \alpha\ \boldsymbol{\nabla} . \dot{\mathbf{u}} + \delta \tilde{p} \frac{\dot{p}}{Q} - \delta \tilde{p}\ \beta_f \dot{\theta} \right) d\Omega = 0 \\
&\int_\Omega \left(- \delta \boldsymbol{\nabla} \tilde{\theta} . \boldsymbol{J}_{\mathrm{dif}} + \delta \tilde{\theta} (\rho c)_f \dot{\mathbf{w}} . \boldsymbol{\nabla} \theta + \delta \tilde{\theta}\ \rho c \dot{\theta} \right) d\Omega = 0
\end{aligned} \tag{17}$$

Applying the finite element discretization, the weak forms of the micro-scale domain can be discretized as

$$\begin{aligned}
\boldsymbol{\psi}_u &= \mathbf{M}_u \ddot{\mathbf{U}} + \mathbf{K}\mathbf{U} - \mathbf{Q}\mathbf{P} - \mathbf{W}\boldsymbol{\Theta} - \mathbf{F}_u = \mathbf{0} \\
\boldsymbol{\psi}_p &= \mathbf{M}_f \ddot{\mathbf{U}} + \mathbf{Q}^{\mathrm{T}} \dot{\mathbf{U}} + \mathbf{H}\,\mathbf{P} + \mathbf{S}\,\dot{\mathbf{P}} + \mathbf{R}\,\dot{\boldsymbol{\Theta}} - \mathbf{F}_p = \mathbf{0} \\
\boldsymbol{\psi}_T &= \mathbf{L}\,\dot{\boldsymbol{\Theta}} + \mathbf{C}\,\boldsymbol{\Theta} - \mathbf{F}_\theta = \mathbf{0}
\end{aligned} \tag{18}$$

in which the complete definition of the matrices and vectors can be found in references [26, 27]. Implementation of the Newton-Raphson linearization method, the system of algebraic equations can be described as

$$\mathcal{F}_n^{i+1} = \mathcal{F}_n^i + \mathcal{J}_n^i . d\mathcal{X}_n^i \quad , \quad \mathcal{F} = \begin{Bmatrix} \boldsymbol{\psi}_u \\ \boldsymbol{\psi}_p \\ \boldsymbol{\psi}_T \end{Bmatrix} \quad , \quad \mathcal{X} = \begin{Bmatrix} \mathbf{U} \\ \mathbf{P} \\ \boldsymbol{\Theta} \end{Bmatrix} \tag{19}$$

Applying the Newmark method for the time domain discretization in equations (18), in which the time derivative variables are expressed in terms of the known variables given in the previous increment and unknown current variables, the microscopic Jacobian matrix can be obtained as

$$\mathcal{J} = \begin{bmatrix} a_0\mathbf{M}_u + \mathbf{K} & -\mathbf{Q} & -\mathbf{W} \\ a_0\mathbf{M}_f + \mathbf{Q}^{\mathrm{T}} & \mathbf{H} + a_6\mathbf{S} & a_6\mathbf{R} \\ \mathbf{0} & \mathbf{0} & a_6\mathbf{L} + \mathbf{C} \end{bmatrix} \tag{20}$$

where $a_0 = 1/(\alpha_2 \Delta t^2)$ and $a_6 = 1/(\alpha_3 \Delta t)$ with α_2 and α_3 denoting the Newmark parameters.

The multiscale analysis is performed using the FE^2 technique, in which the initial and boundary conditions of the real problem are considered for the macro-scale domain. The macro-scale domain is discretized by the finite element method and the relevant matrices are obtained for the medium. An RVE is associated with each Gauss point of an element, as a micro-scale domain, and the field variables are transferred to the discretized micro-scale domain. The nonlinear transient micro-scale problem is solved using the appropriate initial and boundary conditions through the iterative Newton-Raphson method, and the macroscopic variables and tangent operators are extracted from the resultant solution. The quantities are then transferred to the macro-scale domain and utilized in the Newton-Raphson procedure. While the data corresponding to all Gauss integration points in the macro-scale domain are extracted from the micro-scale analyses, the linearized macro-scale equations are solved and the field variables are updated. The above iterative procedure is continued until the convergence is achieved at the macro-scale domain.

5 NUMERICAL SIMULATION RESULTS

In order to demonstrate the efficiency and accuracy of the proposed multiscale algorithm, the coupled thermo-hydro-mechanical analysis is performed for a 2D heterogeneous medium. A square domain of $6 \times 6\,\mathrm{m}^2$ is constructed from two different materials, called the matrix and particle, as shown in Figure 1. The material properties of the matrix and particle are given in Table 1. The particles are considered as a circular shape with the radius of $0.35\,\mathrm{m}$. The geometry and boundary conditions of the problem are presented in Figure 1. The medium is restricted to horizontal displacement at the left and right edges, while the top and bottom edges are constrained against the vertical displacement. In fact, the problem is assumed as one-quarter of an injection-production system, in which the fluid is injected from its center and the production occurs at the corners (see Figure 1). On the other hand, on the virtue of symmetry the above boundary conditions are appropriate for the injection-production problem. It must be noted that the displacement field is not zero within the domain since there are the fluid flow and temperature changes that can affect the displacement field. Moreover, the temperature of $100\,^{\circ}\mathrm{C}$ is applied at the region A, while the temperature of region B is set to zero.

Table 1: Material properties of the square heterogeneous medium

Property	Material 1 (Matrix)	Material 2 (Particle)
Elasticity modulus	$E = 6$ MPa	$E = 3000$ MPa
Poisson ratio	$\nu = 0.4$	$\nu = 0.4$
Biot coefficient	$\alpha = 1$	$\alpha = 0.65$
Porosity	$n = 0.3$	$n = 0.1$
Solid density	$\rho_s = 2000$ Kg/m^2	$\rho_s = 20000$ Kg/m^2
Water density	$\rho_w = 1000$ Kg/m^2	$\rho_w = 1000$ Kg/m^2
Bulk modulus of solid	$K_s = 10^7$ MPa	$K_s = 10^8$ MPa
Bulk modulus of fluid	$K_f = 10^3$ MPa	$K_f = 10^3$ MPa
permeability	$k = 1.1 \times 10^{-9}$ m^4/Pa.s	$k = 3.8 \times 10^{-11}$ m^4/Pa.s
Thermal conductivity of mixture	$\lambda = 837$ W/m C°	$\lambda = 16.74$ W/m C°
Heat capacity of solid	$c_s = 878$ J/kg C°	$c_s = 1369.7$ J/kg C°
Heat capacity of fluid	$c_f = 4184$ J/kg C°	$c_f = 4184$ J/kg C°
Thermal expansion coefficient	0.9×10^{-6}	0.3×10^{-6}

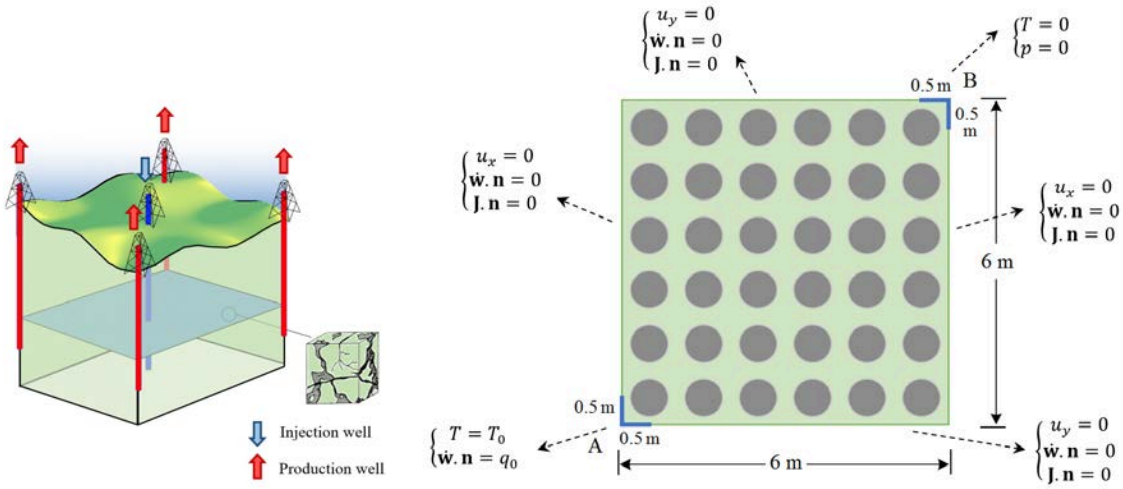

Figure 1: A heterogeneous square domain; The geometry and boundary conditions

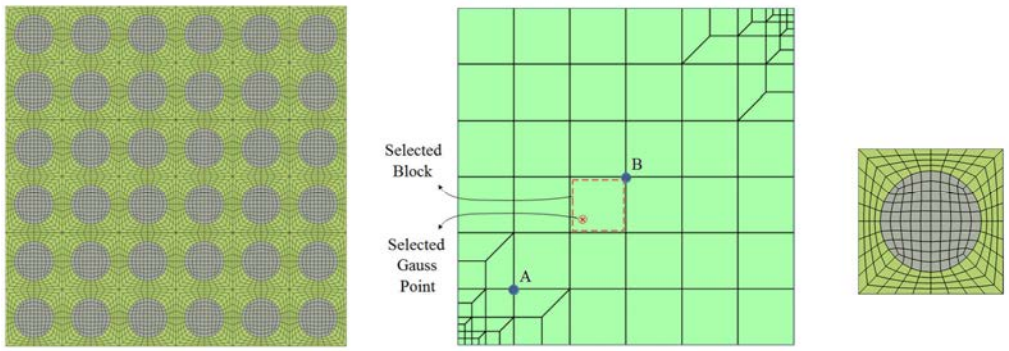

Figure 2: A heterogeneous square domain; a) Finite element mesh of DNS model, b) FE mesh of macro-scale model, c) the RVE of the micro-scale model

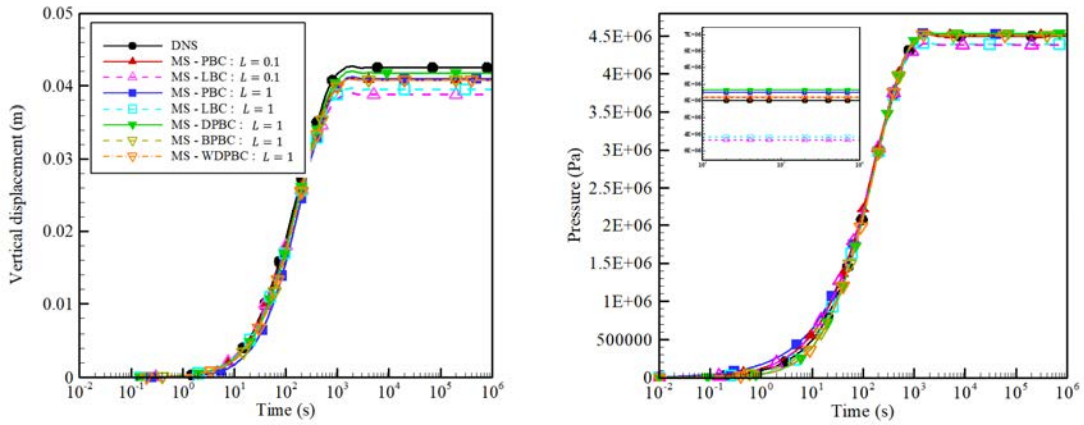

Figure 3. The variations with time of the vertical displacement and fluid pressure for the THM analysis of a heterogeneous square domain at point A; A comparison between the DNS model and multi-scale analysis with different RVE boundary conditions and length scales

The fluid is injected with a rate of $q = 10^{-4}\ \mathrm{m}^2/\mathrm{s}$ from the region A uniformly distributed in $1\,\mathrm{m}$ length ($0.5\,\mathrm{m}$ along each side). Similarly, the pressure is set to zero at the region B as the production area. Other boundaries are insulated to the fluid and heat exchange. The DNS model is performed to compare the results of the multiscale analysis with a very fine FE mesh and to illustrate the accuracy of the method. The FE mesh of DNS model is constructed from 8064 bilinear elements with 8161 nodes, as shown in Figure 2. In this figure, the FE meshes of macro-scale and micro-scale analyses are presented. The macro-scale domain consists of 78 bilinear elements with 103 nodes, and the RVE comprises of 224 elements with 241 nodes. In the multiscale analysis, different aspects of micro-scale boundary conditions are studied, including the typical periodic boundary condition with corner nodes constraints (PBC), periodic boundary condition with domain integral constraint (D–PBC), periodic boundary condition with boundary integral constraint (B–PBC), periodic boundary condition with weighted domain integral constraint (WD–PBC), and linear boundary condition (LBC) using two RVE length sizes of $L = 0.1$ and $1\,\mathrm{m}$.

In Figure 3, the variations with time of the vertical displacement and fluid pressure are plotted for the heterogeneous square domain at point A. Obviously, the results of multiscale analysis using various micro-scale boundary conditions are in good agreement with that obtained from the DNS model. However, a slight discrepancy can be seen in the displacement field using the LBC model with the RVE length sizes of $L = 0.1$ and $1\,\mathrm{m}$ at the steady state condition. In Figure 4, the variations with time of the temperature are plotted for a heterogeneous square domain at points A and B. It can be observed that the results of multiscale analysis with different micro-scale boundary conditions are close to that of DNS model at point B. However, significant discrepancies can be observed for the RVE size of $L = 0.1$ and WD–PBC model at point B. On the other hand, the results of typical PBC with $L = 0.1$ and $1\,\mathrm{m}$ as well as the LBC with $L = 0.1\,\mathrm{m}$, and WD–PBC model are completely unacceptable for point A due to substantial deviations even in large time steps. Unlikely, D–PBC, B–PBC and LBC with $L = 1\,\mathrm{m}$ present a reasonable agreement with the DNS model. Since the idea of boundary integral periodic boundary condition is taken from the linear boundary condition, appropriate results can be expected from these approaches.

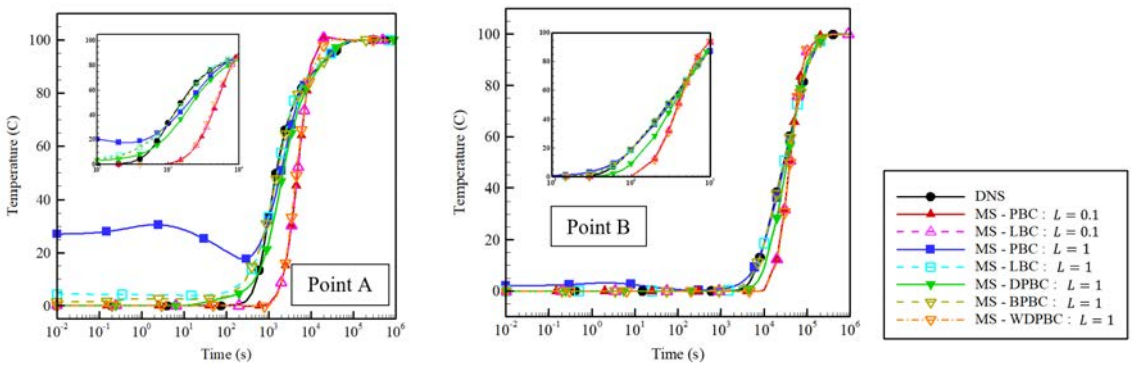

Figure 4. The variations with time of the temperature for the THM analysis of a heterogeneous square domain at points A and B; A comparison between the multiscale analysis with different RVE boundary conditions and RVE length scales

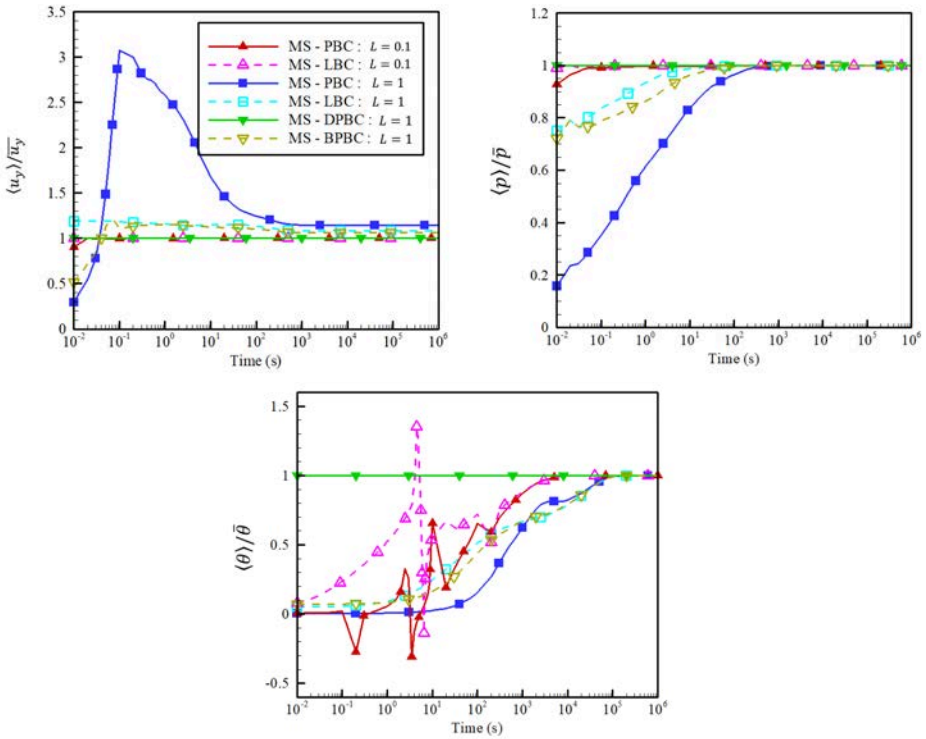

Figure 5. The variations with time of the ratio of average micro-scale field variables to the macro-scale solution at the selected Gauss integration point

In Figure 5, the variations with time of the ratio of average micro-scale field variables to the macro-scale solution are plotted at the selected Gauss integration point. It can be observed that the ratio of average micro-scale to macro-scale solution for the displacement and pressure fields are close to each other for the most micro-scale boundary conditions except the typical PBC model with $L = 1\,\mathrm{m}$. However, the typical PBC experiences deviation from the unity that alerts the possible discrepancy in highly transient problems. Moreover, the ratio of average micro-scale to macro-scale of the thermal field demonstrates completely improper behavior for all micro-scale boundary conditions except the D–PBC model.

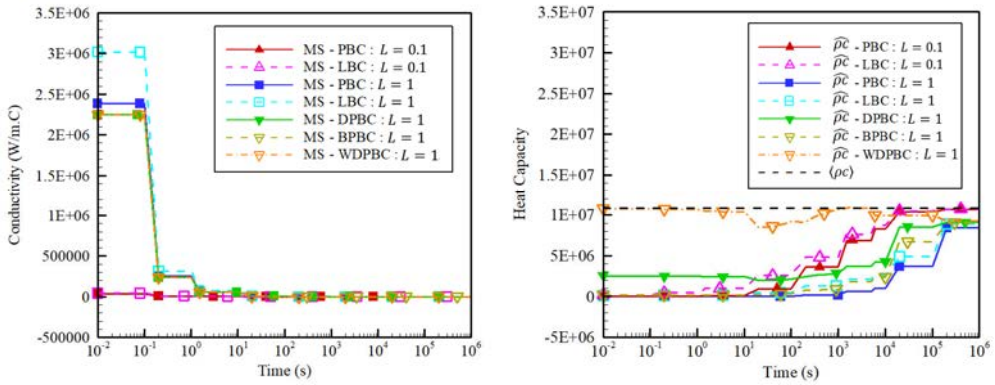

Figure 6. The variations with time of the homogenized conductivity and the heat capacity for the THM analysis of a heterogeneous square domain using multiscale analysis using different RVE boundary conditions and RVE length scales

The oscillating behavior can be even seen in Figure 5 for the LBC and PBC models with $L = 0.1\text{m}$. Although the LBC with $L = 1\text{m}$ and the B–PBC model are far from the unity, the solution is still desirable. It is noteworthy that this ratio explains how the microscopic fluctuation fields vary over the RVE. As the transient terms become larger, the variation of fluctuation fields become intensive, and as a result, the first order homogenization approach fails to yield to the desirable solution. In fact, the larger size of the RVE results in the violation of the principle of separation of scales in transient problems in the case of typical PBC model. In Figure 6, the variations with time of the homogenized conductivity and the heat capacity are plotted for the THM analysis of a heterogeneous square domain using the multiscale analysis with different RVE boundary conditions and RVE length scales. It can be observed that the heat capacity of the LBC and PBC models with $L = 0.1\text{m}$ approach the volume average of corresponding material property, while the other RVE boundary conditions converge to a different value in the steady state condition. In fact, it confirms that the classical assumption of the equivalent heat capacity in the steady-state microscopic solution can be chosen as the volume average of the heat capacity. Moreover, a comparison between the results of homogenized conductivity of the conduction-convection case and the only conduction case reveals that the LBC and PBC models with $L = 0.1\text{m}$ are not affected by the convection phenomenon, while the other RVE boundary conditions except the LBC with $L = 1\text{m}$ converge to the value of 760 $\text{W}/\text{m.C}$ in the steady state condition. In addition, the WD–PBC model presents the oscillating behavior in both the homogenized conductivity and heat capacity. Moreover, the LBC model represents a larger conductivity than the PBC model at early time steps, which is rational due to overestimation manner of the LBC. However, in the steady state condition, the resultant conductivity of PBC model becomes greater than the LBC model. This behavior is the result of convection heat transfer that affects the homogenized conductivity.

6 CONCLUSIONS

In the present paper, a multiscale FE^2 framework was developed for two-scale simulation of the thermo-hydro-mechanical analysis of heterogeneous porous media. The governing equations was presented based on the classical Biot theory of porous media in combination with the advection-diffusion equation as the energy balance equation. The first order homoge-

nization method was applied, in which the main macroscopic field variables and their gradients were downscaled to the micro-scale level. In order to satisfy the Hill-Mandel principle of macro-homogeneity, the proper virtual power relations were defined based on the variational forms of the governing equations as the bridging of the micro- to macro-scale level. The weak forms of the micro-scale governing equations were derived and solved according to the appropriate boundary conditions. Moreover, the transient dynamic terms were included in the micro-scale formulations by defining several additional constraints to the conventional periodic boundary conditions, in order to achieve accurate results in the presence of micro-inertial terms. It was described that the transient effects cannot be captured through the conventional periodic boundary conditions. Furthermore, the Petrov-Galerkin FE^2 method was applied for the advection dominant heat transfer to restrict inaccurate solutions, although the resultant macroscopic field cannot reveal oscillatory behavior. Finally, the capability and accuracy of the proposed computational multiscale algorithm was presented through the coupled thermo-hydro-mechanical analysis of a 2D heterogeneous medium. It was demonstrated that in transient problems, the principle of separation of scales cannot be applied in the computational homogenization method, while the micro-inertial terms were neglected in small RVEs and the inconsistency can be observed with the exact solution. Even more, the inaccuracy of the results was obvious when the convection heat transfer was incorporated. In addition, the D–PBC and B–PBC models illustrate the most promising results comparing to the DNS model.

REFERENCES

[1] R.W. Lewis, C. Majorana, B. Schrefler, A coupled finite element model for the consolidation of nonisothermal elastoplastic porous media. *Transport in Porous Media* **1**, 155–178, 1986.

[2] S. Seetharam, H. Thomas, P.J. Cleall, Coupled thermo/hydro/chemical/mechanical model for unsaturated soils – Numerical algorithm. *International Journal for Numerical Methods in Engineering* **70**, 1480–1511, 2007.

[3] R. Liu, M. Wheeler, C. Dawson, R. Dean, Modeling of convection-dominated thermoporomechanics problems using incomplete interior penalty Galerkin method. *Computer Methods in Applied Mechanics and Engineering* **198**, 912–919, 2009.

[4] A.R. Khoei, T. Mohamadnejad, Numerical modeling of multiphase fluid flow in deforming porous media; A comparison between two- and three-phase models for seismic analysis of earth and rockfill dams. *Computers and Geotechnics* **38**, 142–166, 2011.

[5] W. Cui, K. Gawecka, D. Taborda, D. Potts, L. Zdravković, Time-step constraints in transient coupled finite element analysis. *International Journal for Numerical Methods in Engineering* **106**, 953–971, 2016.

[6] A.R. Khoei, S.M.S. Mortazavi, Thermo-hydro-mechanical modeling of fracturing porous media with two-phase fluid flow using X-FEM technique. *International Journal for Numerical and Analytical Methods in Geomechanics* **44,** 2430–2472, 2020.

[7] J. Rutqvist, L. Börgesson, M. Chijimatsu, A. Kobayashi, et al., Thermo-hydro-mechanics of partially saturated geological media: governing equations and formulation of four finite element models. *International Journal of Rock Mechanics and Mining Sciences* **38**, 105–127, 2001.

[8] A.R. Khoei, D. Amini, S.M.S. Mortazavi, Modeling non-isothermal two-phase fluid flow with phase change in deformable fractured porous media using extended–FEM. *International Journal for Numerical Methods in Engineering* **122**, 4378–4426, 2021.

[9] M. Duflot, The extended finite element method in thermoelastic fracture mechanics. *International Journal for Numerical Methods in Engineering* **74**, 827–847, 2008.

[10] A.R. Khoei, S. Moallemi, E. Haghighat, Thermo-hydro-mechanical modeling of impermeable discontinuity in saturated porous media with X-FEM technique. *Engineering Fracture Mechanics* **96**, 701–723, 2012.

[11] A.R. Khoei, B. Bahmani, Application of an enriched FEM technique in thermo-mechanical contact problems. *Computational Mechanics* **62**, 1127–1154, 2018.

[12] S. Mortazavi, P. Pirmoradi, A.R. Khoei, Numerical simulation of cold and hot water injection into naturally fractured porous media using XFEM and an equivalent continuum model. *International Journal for Numerical and Analytical Methods in Geomechanics* **46**, 617–655, 2022.

[13] M.V. Júnior, E.A. de Souza Neto, P.A. Munoz-Rojas, *Advanced Computational Materials Modeling: from Classical to Multiscale Techniques*. John Wiley 2011.

[14] V.P. Nguyen, O. Lloberas-Valls, M. Stroeven, L.J. Sluys, On the existence of representative volumes for softening quasi-brittle materials – a failure zone averaging scheme. *Computer Methods in Applied Mechanics and Engineering* **199**, 3028–3038, 2010.

[15] A.R. Khoei, M.R. Hajiabadi, Fully coupled hydro-mechanical multiscale model with micro-dynamic effects. *International Journal for Numerical Methods in Engineering* **115**, 293–327, 2018.

[16] M.G. Geers, V.G. Kouznetsova, W. Brekelmans, Multiscale computational homogenization: Trends and challenges. *Journal of Computational Applied Mathematics* **234**, 2175–2182, 2010.

[17] A. Waseem, T. Heuze, L. Stainier, M. Geers, V. Kouznetsova, Model reduction in computational homogenization for transient heat conduction. *Computational Mechanics* **65**, 249–266, 2020.

[18] K. Pham, V. Kouznetsova, M.G. Geers, Transient computational homogenization for heterogeneous materials under dynamic excitation. *Journal of the Mechanics and Physics of Solids* **61**, 2125–2146, 2013.

[19] R.W. Lewis, B. Schrefler, *The Finite Element Method in the Static and Dynamic Deformation and Consolidation of Porous Media*. John Wiley 1998.

[20] O.C. Zienkiewicz, R.L. Taylor, P. Nithiarasu, *The Finite Element Method for Fluid Dynamics*. Elsevier 2014.

[21] A.R. Khoei, *Extended Finite Element Method, Theory and Applications*. John Wiley 2015.

[22] A. Waseem, T. Heuzé, L. Stainier, M. Geers, V. Kouznetsova, Two-scale analysis of transient diffusion problems through a homogenized enriched continuum. *European Journal of Mechanics A. Solids* **87**, 104212, 2021.

[23] H.J.G. Diersch, *FEFLOW: Finite Element Modeling of Flow, Mass and Heat Transport in Porous and Fractured Media*. Springer 2013.

[24] I. Özdemir, W. Brekelmans, M. Geers, Computational homogenization for heat conduction in heterogeneous solids. *International Journal for Numerical Methods in Engineering* **73**, 185–204, 2008.

[25] E. de Souza Neto, P. Blanco, P. Sánchez, R. Feijóo, An RVE-based multiscale theory of solids with micro-scale inertia and body force effects. *Mechanics of Materials* **80**, 136–144, 2015.

[26] A.R. Khoei, S. Saeedmonir, Computational homogenization of fully coupled multiphase flow in deformable porous media. *Computer Methods in Applied Mechanics and Engineering* **376**, 113660, 2021.

[27] S. Saeedmonir, A.R. Khoei, Multiscale modeling of coupled thermo-hydro-mechanical analysis of heterogeneous porous media. *Computer Methods in Applied Mechanics and Engineering* **391**, 114518, 2022.